INVESTIGATION OF PROGRESSIVE AND ULTIMATE FAILURE FOR WOVEN-FABRIC COMPOSITE STRUCTURES

L. Dong, [1] and J. Blachut [2]

[1]*School of Mechanical and Materials Engineering, The University of Surrey, Guildford, Surrey GU2 5XH, UK.*
[2] *Mechanical Engineering, The University of Liverpool, Liverpool, L69 3GH, UK.*

SUMMARY
The paper describes behaviour of torispherical shells, made from multi-ply and non-cut draped woven carbon fabric, subjected to uniform external pressure. The fishnet algorithm was used for simulation of woven fabric drape on doubly curved surfaces. The resulting local fibre orientation and variable wall thickness were used in the subsequent computations. The progressive failure anlysis was carried out using finite element method in which the interactive Tsai-Wu stress failure criterion with a stiffness reduction scheme was adopted. The effect of inter-laminar shear strength on the collapse load is included. The effect of unsymmetrically draped fabric on the failure load of domes is also investigated. Details are provided about the experimental work, in which 10 carbon fibre domes with up to 56 plies were manufactured and collapsed by external pressure in the range between 7 MPa and 29 MPa.

KEYWORDS: progressive failure, draping, computational modelling, woven fabric, external pressure, collapse, torispheres.

INTRODUCTION

Structural composite components made from textile fabric can be found in many engineering applications. Different manufacturing techniques need to be used to manufacture these components since many of them cannot be, for example, filament wound due to shape constraints. Alternative techniques include hand lay-up, resin transfer moulding or vacuum assisted resin infusion [1,2]. For axisymmetric shells like torispherical domed closures in pressure vessels it seems that filament winding would be a natural method of manufacturing. In practice it turned out very difficult to wind a torispherical end closure, without any internal liner or openings and, which could withstand a large external pressure. Hand lay-up of woven fabric was therefore tried successfully as an alternative manufacturing route. The domes were subsequently collapsed by quasi-static external pressure [3]. In all follow-up work the wall thickness-to-diameter ratio was such that the failure mode was associated with collapse rather than with static stability, i.e. bifurcation buckling. Prediction of the ultimate

load carrying capacity for the above mentioned shells poses several difficulties and some aspects of numerical calculations are still guess work. Firstly, a domed pressure vessel end closure is an axisymmetric, doubly curved shell. A ply draped from flat woven fabric to a torispherical geometry, although geometrically axisymmetric, has a non-axisymmetric material properties. The local orientation of draped fabric usually changes from point to point and from layer to layer in components which are not flat. The wall thickness is also affected by the draping process and this is especially true for doubly curved structures, i.e. for domed end closures in pressure vessels. The ability to model the fabric's distortion caused by draping and the ability to predict the wall thickness distribution, also caused by draping, are the necessary requirements for accurate failure analysis of these shells. The stacking sequence of plies with variable thickness and plies with distorted woven grid due to draping create an added modelling difficulty. A number of different approaches were tried in the past to address the above aspects of modelling. Details can be found in Refs. [4,5].
This paper summarises numerical and experimental results for 10 torispherical domes made from draped woven carbon pre-preg and collapsed by quasi-static external pressure. Both First Ply Failure (FPF) pressure and Last Ply Failure Pressure (LPF) are calculated. The effect of interlaminar shear strength on the ultimate collapse pressure is also assessed.

PRELIMINARIES

Let us consider a section through torispherical shell, as sketched in Fig. 1. The shell's geometry is given by radius of the spherical portion, R_s , radius of the toroidal section, r, and diameter D. These dimensions refer to the outer surface. An integral cylindrical flange has length, L, and the wall thickness varies both along the meridian and circumference. All shells discussed in this paper were manufactured by hand lay-up in a female moulding tool. Each ply was made from a non-cut fabric and layers were differently stacked as detailed later. The initially flat and orthogonal woven grid becomes distorted during the drape as sketched in Fig. 2a where one quadrant is draped over a torispherical geometry. It is seen from Fig. 2a that the grid distortion becomes progressively larger in the knuckle and

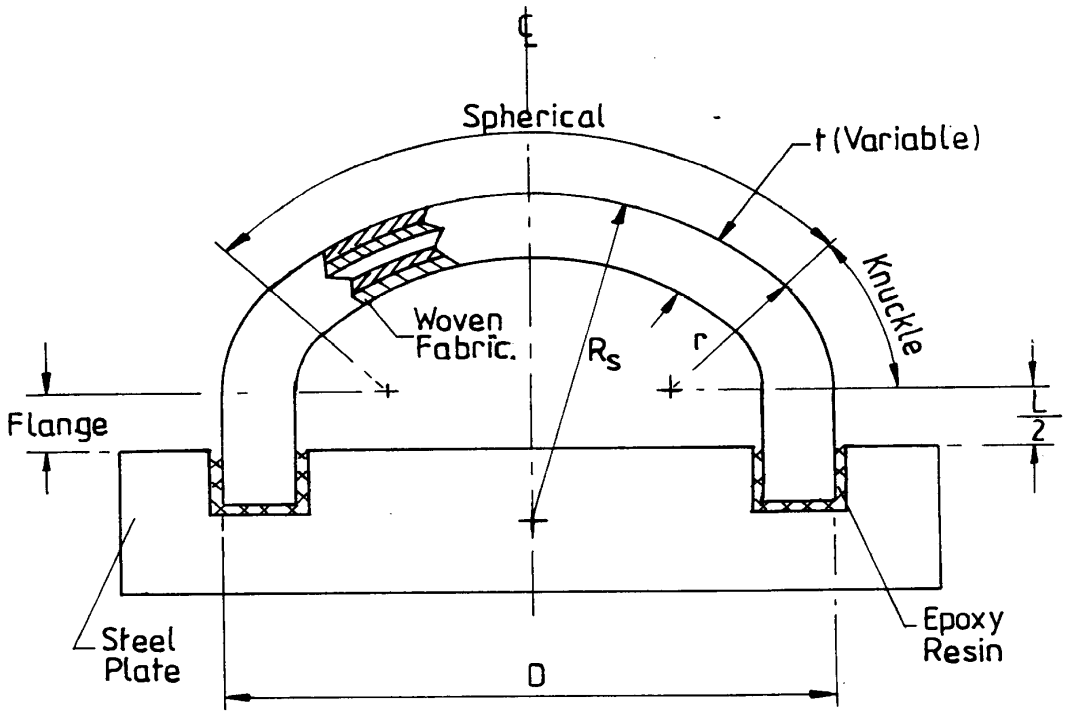

Fig. 1 Geometry of a composite torisphere. Note that all parameters are related to the outer surface.

Table 1: Geometry of external surface and average wall thickness of spherical, knuckle and cylindrical segments. Values in brackets denote the standard deviations.

Dome	r (mm)	R_s (mm)	D (mm)	L (mm)	t_{sph} (mm)	t_{knk} (mm)	t_{cyl} (mm)	t_{apex} (mm)
SVB1	45.0 (0.14)	300.5 (0.25)	299.6 (0.10)	51.3	15.40 (0.08)	15.74 (0.26)	18.25 (1.26)	15.51
SVB1A	45.0 (0.15)	302.5 (0.19)	299.7 (0.11)	51.3	15.11 (0.06)	15.69 (0.46)	18.06 (0.89)	15.19
SVB2	45.13 (0.14)	300.5 (0.20)	299.6 (0.12)	51.6	14.92 (0.05)	15.46 (0.42)	17.75 (1.53)	14.88
SVB2A	45.07 (0.06)	300.2 (0.25)	299.5 (0.04)	51.7	15.32 (0.07)	15.84 (0.43)	18.17 (1.73)	15.25
SVB3	45.0 (0.15)	301.1 (0.31)	299.5 (0.13)	51.7	15.74 (0.06)	16.28 (0.47)	18.69 (2.08)	15.73
SVB3A	45.0 (0.08)	300.9 (0.44)	299.5 (0.04)	51.3	15.35 (0.10)	15.95 (0.57)	18.34 (2.24)	15.36
SVB4	45.07 (0.06)	299.6 (0.25)	299.6 (0.03)	51.2	16.92 (0.07)	17.52 (0.51)	20.29 (1.59)	16.78
SVB4A	44.76 (0.06)	300.9 (0.25)	299.6 (0.04)	51.7	16.81 (0.08)	17.28 (0.48)	19.92 (1.55)	16.76
SVB11	44.67 (0.05)	300.8 (0.78)	299.4 (0.09)	49.8	5.50 (0.07)	5.84 (0.25)	6.58 (0.48)	5.63
SVB11A	45.59 (0.07)	300.4 (0.73)	299.7 (0.07)	49.9	5.73 (0.06)	5.99 (0.21)	6.79 (0.53)	5.71

Table 2: Details about the stacking sequence, number of plies, position of the Focal Point and adopted instrumentation during testing (sym ≡ symmetrical).

Dome	Stacking Sequence (in degrees)	No. of ply	Focal Point	On-line monitoring	Strain gauges
SVB1	$\{[0/60/-60]_8/0\}_{sym}$	50	apex	no	no
SVB1A	$\{[0/60/-60]_8/0\}_{sym}$	50	apex	yes	no
SVB2	$\{[0/45/-45/90]_6/0\}_{sym}$	50	apex	yes	yes
SVB2A	$\{[0/45/-45/90]_6/0\}_{sym}$	50	apex	yes	yes
SVB3	$[0/5/10/15/20/25/30/35/40/45]_5$	50	apex	yes	yes
SVB3A	$[0/5/10/15/20/25/30/35/40/45]_5$	50	off-axis	yes	no
SVB4	$\{[0/60/-60]_9/0\}_{sym}$	56	apex	yes	yes
SVB4A	$\{[0/60/-60]_9/0\}_{sym}$	56	apex	yes	no
SVB11	$\{[0/60/-60]_3\}_{sym}$	18	apex	yes	no
SBVB11A	$\{[0/60/-60]_3\}_{sym}$	18	off-axis	yes	no

cylindrical segments. In the end, a portion of the cloth has to be trimmed and discarded. The fishnet algorithm is capable of predicting the net layout of initially flat fabric in such a way that after the drape there is no need for trimming. This can be clearly seen in Fig. 2b and also in Fig. 3. The algorithm itself is outlined in Ref. [5] Details about geometry of 10 domes considered in this paper are provided in Table 1. The same moulding tool was used for all

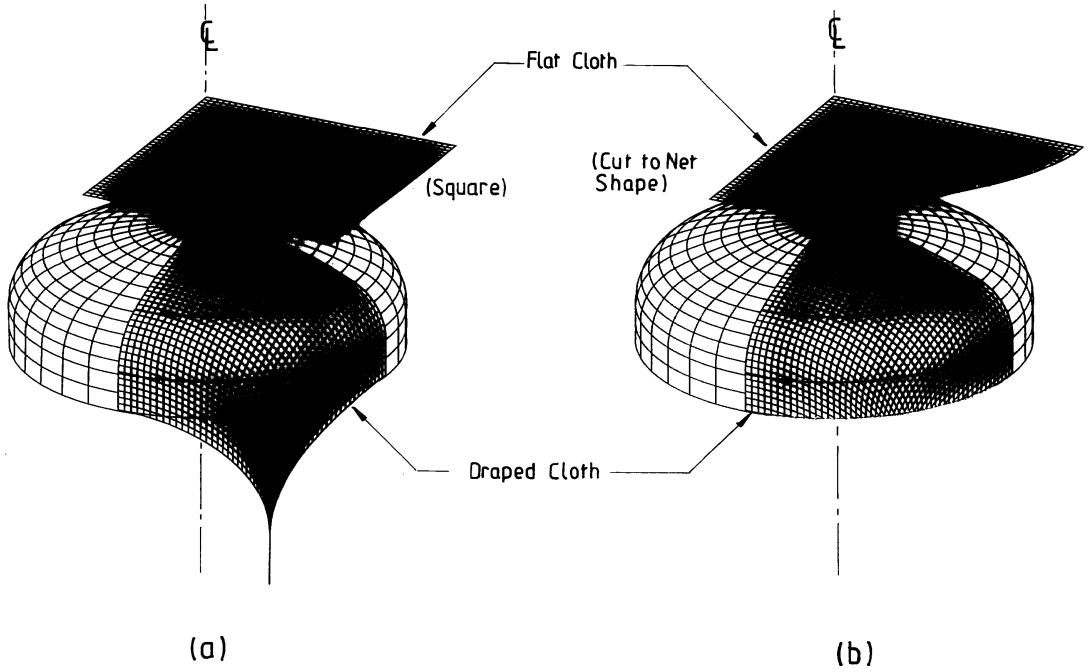

Fig. 2 Numerically simulated distortion of a single-ply, square piece of woven fabric when draped onto torispherical geometry. Note: Focal Point at apex.

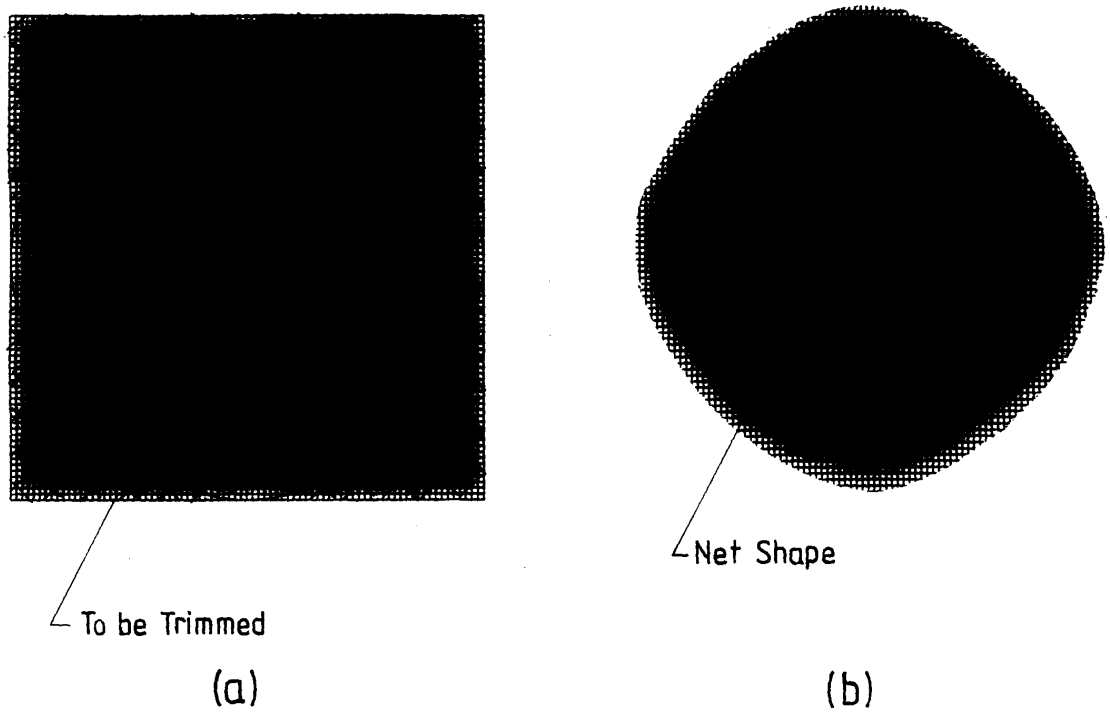

Fig. 3 The amount of fabric which needs to be trimmed after draping a square piece into a torispherical shape (Fig. 3a). Net shape of flat fabric which does not need any trimming after draping (Fig. 3b).

shells hence the geometry of the outer surface is nominally the same. Various stacking sequences, number of plies and various positions of the Focal Point were used during the manufacturing process and this data is summarised in Table 2.

Table 3: Minimum, average and maximum elastic properties for CFRP laminate.

Material Properties	E_{11}	E_{22}	G_{12}	ν_{12}
	(GPa)			
Minimum:	55.83	55.83	3.52	0.07
Average:	60.0	60.0	3.80	0.07
Maximum:	70.11	70.11	4.03	0.07

FIRST PLY AND PROGRESSIVE FAILURE ANALYSIS

It is important to designers to know the ultimate collape load of a structure in order to assess the residual strength available in that component beyond the first ply failure load. Simulation of the progressive failure, which leads to the final collape load, is therefore nessesary for this purpose. In this paper the woven fabric is assumed to be a solid continuum sheet with linear elastic anisotropic properties. The local fibre orientation is determined by the draping analysis module. The stress-strain analyses are performed using the FE computer code

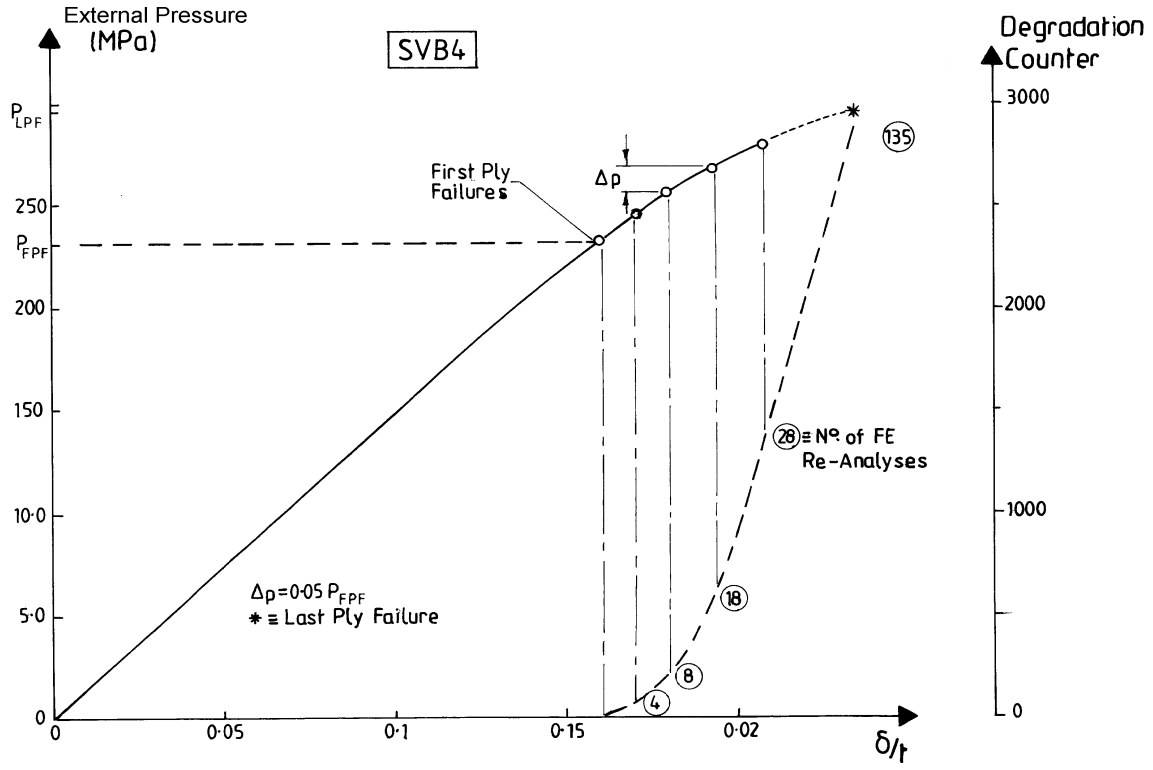

Fig. 4 History of pressure versus apex deflection in 50-ply torisphere. Number of structural re-analyses required per single pressure increment are circled. History of stiffness degradation, in the post-FPF pressure range, is also depicted.

ABAQUS/Standard. A typical finite element model, with eight-node shell elements SR8, is shown in Fig. 2. Results of each FE analysis are post-processed by a separate collapse analysis module. When the first ply failure pressure is found, a small increment of pressure is added and FE analysis is re-run. The over-stressed Gauss Points are degraded and re-analysis of the structure under the same pressure is carried out until no further over-stressing is found. Only then the new increment is added to the pressure. This procedure is repeated until either through the thickness failure occurs or a convergent solution could not be obtained. Further details about this procedure can be found in Refs. [4,5]. Typical plot of external pressure versus apex deflection is shown in Fig. 4 for dome SVB4. The stiffness degradation starts once the FPF pressure is exceeded. The 'Degradation Counter', seen in Fig. 4, shows the total number of times the stiffness was reduced, in both weft and warp fibre directions, at the over-stressed Gauss Points.

The Tsai-Wu interactive failure criterion which is used here has the following form:

$$F_{11}\sigma_1^2 + 2F_{12}\sigma_1\sigma_2 + F_{22}\sigma_2^2 + F_{ss}\sigma_{12} + F_1\sigma_1 + F_2\sigma_2 + F_{st}(\sigma_{13}^2 + \sigma_{23}^2) = 1.0 \qquad (1)$$

where various constants are given by:

$$F_{11} = \frac{1}{X_t X_c}; \quad F_{22} = \frac{1}{Y_t Y_c}; \quad F_1 = \frac{1}{X_t} - \frac{1}{X_c}; \quad F_2 = \frac{1}{Y_t} - \frac{1}{Y_c}; \quad F_{ss} = \frac{1}{S^2};$$

$$F_{12} = -\frac{1}{2}\frac{1}{\sqrt{X_t X_c Y_t Y_c}}; \quad F_{st} = \frac{1}{S_{ILSS}^2}; \tag{2}$$

The compressive strength in the warp and weft directions were taken as $X_C = Y_C = 570$ MPa. The corresponding tensile values were $X_t = Y_t = 600$ MPa whilst the in-plane shear strength S = 50 MPa. The interlaminar shear strength S_{ILSS} is based on published results in Refs. [6-8] and S_{ILSS} = 90 MPa was arbitrarily assumed. The elastic properties were evaluated experimentally using flat test pieces manufactured concurrently with the shells and further details are provided in Ref. [5]. Table 3 gives the minimum, average and the maximum values of elastic properties for the laminate considered in the paper.

Table 4: Effect of net size on the FPF and LPF pressures. Results are shown for dome SVB2A and they are for $E_{11} = E_{22} = 60$ GPa, $G_{12} = 3.86$ GPa and $\nu = 0.07$. The size of flat cloth is 208.6 mm x 208.6 mm. ILSS was not included in the calculations.

	Assumed number of net cells in a flat and square cloth						
Pressure (MPa)	10	20	30	40	60	80	100
p_{FPF}	19.73	20.80	20.92	20.98	21.05	21.06	21.58
$p_{0.05FPF}$	23.88	24.96	25.10	24.13	24.20	24.22	24.22
p_{LPF}	24.47	25.18	25.94	25.65	26.30	25.69	26.16

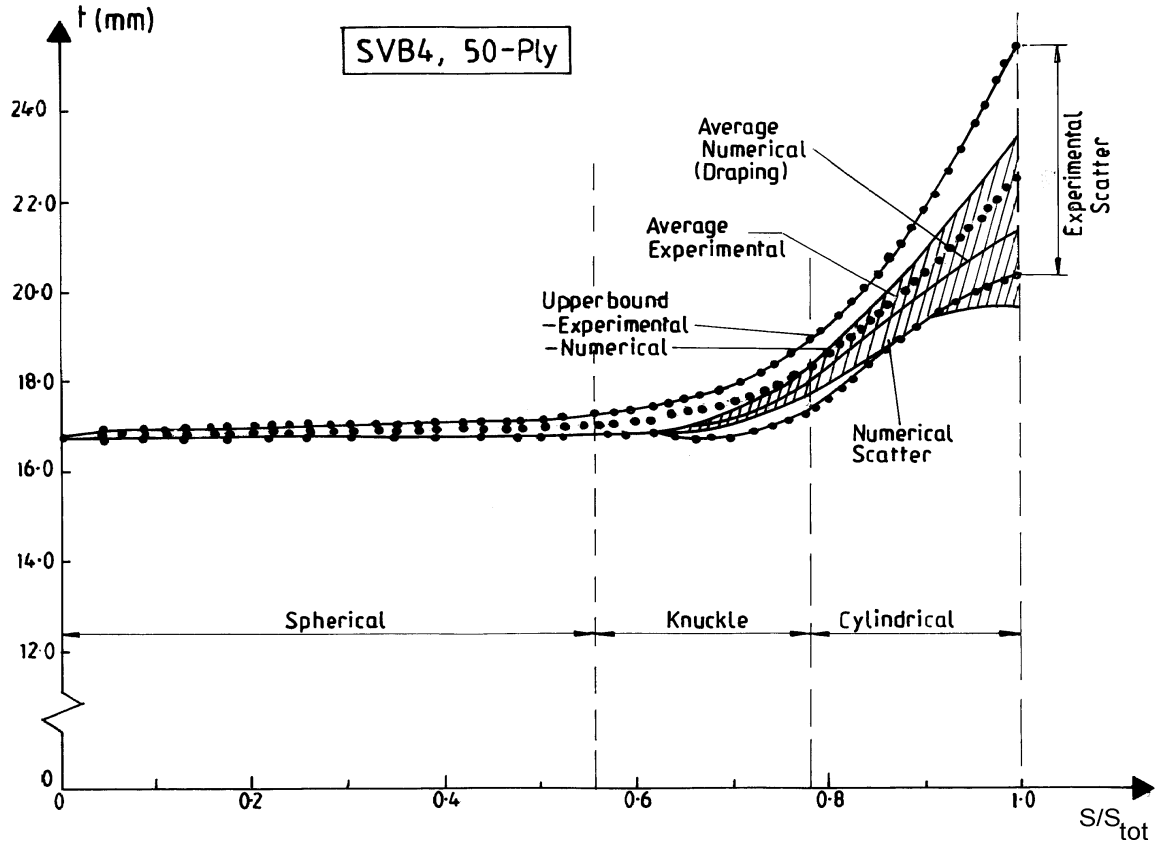

Fig. 5 Comparison of numerically predicted and experimentally measured wall thickness of 50-ply dome.

Table 5: Computed values of the first ply failure pressure and last ply failure pressure for the minimum, average and maximum values of elastic material data obtained in the uniaxial tensile tests of flat samples. The value of the interlaminar shear strength was assumed as S_{ILSS} = 89.6 MPa.

Dome	Material Properties	p_{FPF}	$p_{0.05FPF}$	p_{LPF}
		(MPa)		
SVB2A	Minimum	20.85	23.98	24.40
	Average	21.02	23.13	25.12
	Maximim	21.21	24.46	25.90
SVB3	Minimum	19.11	25.80	27.18
	Average	19.23	25.36	27.42
	Maximum	19.34	27.08	27.66
SVB3A	Minimum	18.41	23.01	23.93
	Average	18.55	23.19	24.12
	Maximum	18.56	24.07	25.40
SVB4	Minimum	23.08	27.70	29.08
	Average	23.25	27.90	29.34
	Maximum	23.29	27.98	30.32

NUMERICAL AND EXPERIMENTAL RESULTS

Several benchmarking computations were carried out in order to assess the influence of various parameters on the load carrying capacity of considered composite domes. This included size of woven net, scatter in material data, etc.

The draping algorithm requires specification of woven cell size. Since the fabric was of 4x4 twill pattern it was assumed that cell's shape should be modelled as a square. A number of different sizes were used to benchmark computations. The influence of the cell size on the FPF and LPF pressures is given in Table 4. It is seen here that for a 50-ply dome the magnitude of the FPF and LPF pressures is only marginally dependent on the size of the drape cell. As a consequence, in all of the ensuing calculations the net size corresponding to 40 cells per square quadrant of fabric was adopted. The wall thickness was measured experimentally at 10 mm intervals along 36 equally spaced meridians. At the same time the wall thickness was predicted using the fishnet algorithm. Comparison of both experimental and numerical values is shown in Fig. 5 where it is seen that the numerical prediction closely follows the experimentally measured thickness profile.

Due to large scatter of experimental material properties (see Table 3), it was decided to evaluate their influence on the FPF and LPF pressures for several different stacking sequences. The obtained results are summarised in Table 5 where the difference between results corresponding to minimum and maximum values of elastic constants is not greater than 6 %. The effect of interlaminar shear on the FPF and LPF loads has also been assessed. Results are given in Table 6. The FPF pressures are not affected by the inclusion of the interlaminar shear strength whilst the LPF pressures are marginally reduced with 4% reduction being the largest value.

All domes were collapsed by quasi-static external pressure in a 0.4 m x 1.5 m pressure chamber. Prior to testing shells were fixed to a 90 mm thick steel base plate as sketched in Fig. 1. Details about the instrumentation can be found in Ref. [5]. Experimental values of collapse pressure are given in the last column of Table 6. The ratio of experimental collapse pressure to computed collapse pressure, i.e. LPF pressure, varies from p_{expt}/p_{num} = 0.90 to p_{expt}/p_{num} = 1.07. Some of tested torispheres were fitted with resistive foil strain gauges mounted on the inside surface. Experimental values of meridional and circumferential

Table 6: Comparison of numerical predictions with the test data. Two sets of numerical results are given, i.e. with and without the Interlaminar Shear Strength (ILSS) being included in the failure criterion given by Eq. (1).

	ILSS = 0.0			ILSS = 90.0 MPa			
	p_{FPF}	$p_{0.05FPF}$	p_{LPF}	p_{FPF}	$p_{0.05FPF}$	p_{LPF}	p_{expt}
Dome	MPa						
SVB1	20.17	24.20	26.34	-	-	-	26.55
SVB1A	19.73	23.67	26.24	19.16	22.99	25.32	25.66
SVB2	18.38	22.98	24.56	-	-	-	25.17
SVB2A	20.98	24.13	25.65	21.03	23.13	25.10	25.59
SVB3	19.23	25.96	27.68	19.23	25.96	27.58	24.83
SVB3A	18.55	23.19	24.24	18.55	23.19	24.12	24.83
SVB4	23.27	27.98	30.13	-	-	-	29.31
SVB4A	22.81	27.38	30.21	23.25	27.90	29.34	28.97
SVB11	4.80	5.76	6.13	4.79	5.75	6.11	6.90
SVB11A	5.03	6.29	6.59	4.92	6.16	6.46	7.06

surface strains are plotted in Fig. 6 as a function of applied pressure. The gauges were mounted at the same distance from the apex and in an isotropic dome they should indicate the same level of straining. Due to anisotropy and varied wall thickness around the circumference, at the same latitude, a sizeable strain difference occurs between the gauges. Despite this, domes failed by through the wall crack running circumferentially along the spherical cap/knuckle junction (see Ref. [5]).

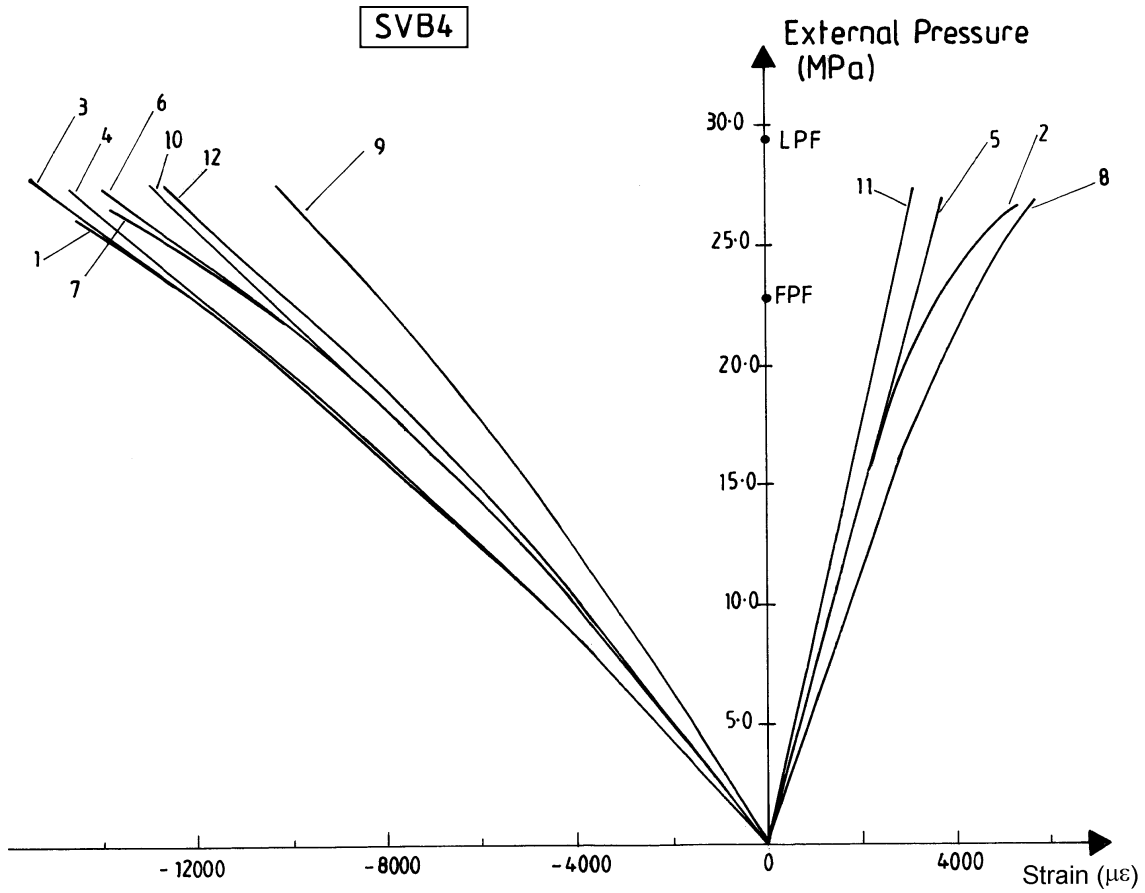

Fig. 6 Plot of pressure versus circumferential (gauges: 1,3,4,6,7,9,10,12) and meridional (gauges: 2,5,8,11) strains obtained form surface bonded foil gauges in 50-ply torisphere.

CONCLUSIONS

The fishnet algorithm proved to be a useful tool in several respects. Firstly, it predicted local fibre orientations - a quantity which is necessary for accurate evaluation of stresses and strains in woven fabric. Secondly, the algorithm was capable of predicting a net shape. This leads to the elimination of trimming, i.e. unnecessary waste of fabric. Another useful quantity, which the fishnet algorithm is capable of, is predicting the wall thickness.

Application of detailed modelling resulted in a good correlation between the predicted Last-Fly-Failure pressures and the experimental collapse pressures for a range of tested torispheres made from carbon/epoxy woven cloth. The ratio of LPF pressure to FPF pressure varies from 1.28 to 1.44. The large ratio of the LPF to the First-Ply-Failure pressure indicates that it is important for the progressive failure analyses to be carried out in order to assess the margin for the ultimate load bearing capacity of domed shells.

REFERENCES

1. H.B. Dexter, “Innovative textile reinforced composite materials for aircraft structures”, in ‘Proc. of 28th International SAMPE Technical Conf.’, (eds) J.T. Hoggat et al, vol. 28, 1996, pp. 404-416.

2. P. Tan, L. Tong, G.P. Steven, “Modelling for predicting the mechanical properties of textile composites - a review”, *Composites Part A*, vol. 28A, 1997, 902-922.

3. J. Blachut, G.D. Galletly, A.G. Gibson, “CFRP domes subjected to external pressure”, *Marine Struct.*, vol. 3, 1990, 149-173.

4. J. Blachut, L. Dong, “Use of woven CFRP for externally pressurised domes”, *Composite Struct*., vol. 38, 1997, 553-563.

5. L. Dong, J. Blachut, “Analysis and collapse of thick composite torispheres”, *Proc. IMechE, Part E,* vol. 212, 1998, 103-117.

6. J. Harding, L. Dong, “Effect of strain rate on the interlaminar shear strength of carbon fibre reinforced laminates”, *Composites Sci. and Technology*, vol. 51, 1994, 347-358.

7. L. Dong, J. Harding, “A single-lap shear specimen for determining the effect of strain rate on the interlaminar shear strength of carbon fibre-reinforced laminates”, *Composites*, vol. 25, 1994, 129-138.

8. M.R. Wisnom, T. Reynolds, N. Gwilliam, “Reduction in interlaminar shear strength by discrete and distributed voids”, *Composites Sci. and Technology*, vol. 56, 1996, 93-101.